Characterization of Photoelectric Properties and Composition Effect of $TiO_2/ZnO/Fe_2O_3$ Composite by Combinatorial Methodology

Yichuan Liao, Huayao Li, Yuan Liu, Zhijun Zou, Dawen Zeng, and Changsheng Xie*

State Key Laboratory of Material Processing and Die & Mold Technology, Nanomaterial and Smart Sensor Research Laboratory, Department of Materials Science and Engineering, Huazhong University of Science and Technology, Wuhan 430074, P.R. China

Received July 2, 2010

On the basis of combinatorial methodology and the idea of an equilateral ingredient triangle, the $TiO_2/ZnO/Fe_2O_3$ composite system including 66 ingredient points was designed. The photocurrents under different light sources and bias voltages were measured, and the photocurrent amplitude at 300 s was chosen as a parameter to evaluate the photoelectric response of the composite. To appraise the composition effect of the composite compared with pure materials, the quantitative formula of the composition effect has been provided for the first time in this paper. We found that not all the ingredient points demonstrated the enhanced composition effect in the as-designed ingredient triangle material library. The reasons of different composition effect for different ingredient points have been discussed in detail. X-ray diffraction (XRD) and field emission scanning electron microscopy (FE-SEM) were used to investigate the phase structure and the grain morphology of the composite.

1. Introduction

Photogenerated electron−hole pairs within the semiconductor could degrade pollutants into non-toxic or less toxic substances.[1−4] To degrade pollutants efficiently, photocatalysts with high activity are needed. The major solution is to improve the yield of photogenerated electron−hole pairs greatly, and to suppress the recombination of them efficiently. The composition of different materials was a promising method to achieve efficient separation of the photogenerated charges in photocatalytic materials and to improve the catalytic activity of the photocatalysts.[5−8] It was reported that TiO_2/CdS composite displayed a considerable improvement in photocatalytic activity and photocurrent relative to pure TiO_2 and CdS.[9] $TiO_2/Fe_2O_3/La_2O_3$ composite significantly raised the photodegradation property of methyl orange compared with pure TiO_2.[10] The photocatalytic activity of the composite of TiO_2 nanoparticles and carbon nanotubes markedly increased by a factor of approximately 2.2 in comparison with pure TiO_2.[11] Nevertheless, whether the composite material at all component proportions could achieve enhanced effect than pure materials is worth thinking over, and, it may not bring about a positive effect at some component proportions. Then, how to evaluate the composition effect of the composite material needs to be carefully analyzed. As can be seen from the present publications, even though much work has been done on photocatalysis of composite materials, there is no general standard with which to judge qualitatively the composition effect of the composite material in contrast with pure materials. Therefore, a reference criterion for the evaluation of the composition effect of the composite material is needed urgently. The method of the combinatorial would be helpful to solve the problem, which could vastly improve the overall efficiency of screening and optimizing composite materials with elevated composition effect.[12−14]

In view of the issue mentioned above, on the basis of combinatorial and the idea of an equilateral ingredient triangle, $TiO_2/ZnO/Fe_2O_3$ composite system which consisted of 66 ingredient points was designed. Photoelectric property measurement was selected to evaluate the photoelectric response capability of the composite. To assess the composition effect of the composite material, the quantitative formula of composition effect has been provided for the first time in this paper, which will be conducive to the design and evaluation of the composite material. The composition effect of different ingredient points in the $TiO_2/ZnO/Fe_2O_3$ composite is discussed in detail, which would be of great significance for the design of the composite for photocatalytic degradation of pollutants.

2. Experimental Section

2.1. Design of Material Library. On the basis of the idea of the equilateral ingredient triangle of the ternary-phase diagram, each side of the triangle was divided into 10 equal portions; thus a material library consisted of 66 ingredient points was obtained. TiO_2, ZnO, and Fe_2O_3 were chosen as the vertex materials of the triangle. The mass of each ingredient point was 20 g. The corresponding device number and mole ratio of each ingredient point was displayed in Table 1. The more details of the design of the material library is found in our previous work.[15] Several reasons were considered for the selection of TiO_2, ZnO, and Fe_2O_3. TiO_2 was used because it has a band gap of 3.2 eV, and relatively

* To whom correspondence should be addressed. E-mail: csxie@mail.hust.edu.cn. Phone: +86-27-8755-6544. Fax: +86-27-8754-3778.

10.1021/cc100121d
Published on Web 09/21/2010

Table 1. Device Number and Mole Ratio of 66 Ingredient Points

ingredient (device) number	TiO_2:ZnO:Fe_2O_3 (mol ratio)	ingredient (device) number	TiO_2:ZnO:Fe_2O_3 (mol ratio)	ingredient (device) number	TiO_2:ZnO:Fe_2O_3 (mol ratio)
1	10:0:0	23	7:1:2	45	0:6:4
2	9:1:0	24	6:2:2	46	5:0:5
3	8:2:0	25	5:3:2	47	4:1:5
4	7:3:0	26	4:4:2	48	3:2:5
5	6:4:0	27	3:5:2	49	2:3:5
6	5:5:0	28	2:6:2	50	1:4:5
7	4:6:0	29	1:7:2	51	0:5:5
8	3:7:0	30	0:8:2	52	4:0:6
9	2:8:0	31	7:0:3	53	3:1:6
10	1:9:0	32	6:1:3	54	2:2:6
11	0:10:0	33	5:2:3	55	1:3:6
12	9:0:1	34	4:3:3	56	0:4:6
13	8:1:1	35	3:4:3	57	3:0:7
14	7:2:1	36	2:5:3	58	2:1:7
15	6:3:1	37	1:6:3	59	1:2:7
16	5:4:1	38	0:7:3	60	0:3:7
17	4:5:1	39	6:0:4	61	2:0:8
18	3:6:1	40	5:1:4	62	1:1:8
19	2:7:1	41	4:2:4	63	0:2:8
20	1:8:1	42	3:3:4	64	1:0:9
21	0:9:1	43	2:4:4	65	0:1:9
22	8:0:2	44	1:5:4	66	0:0:10

strong photocatalytic activity and biological and chemical stability.[16] ZnO was chosen on account of its wider absorption spectrum of the sunlight than TiO_2, and its band gap is 3.2 eV.[16] Fe_2O_3 was selected because its band gap is 2.2 eV which could absorb both ultraviolet and part of visible light in theory.[16] They were both non-toxic and low price. Since a band gap gradient with different energy levels was formed among the TiO_2/ZnO/Fe_2O_3 composite, an effective separation of photogenerated charges may occur among the contacting particles, and the composite may realize the total response to the solar spectrum; therefore it may show a heightened photoelectric composition effect.

2.2. Device Preparation. TiO_2 (Degussa P25, average grain size: 30 nm), ZnO (average grain size: 100 nm), Fe_2O_3 (α-Fe_2O_3, average grain size: 30 nm), and other chemicals used in the experiment were of analytically pure grade. All of them were used as received without any pretreatment. Ball milling was used to homogeneously mix the three kinds of powders and a certain amount of organic solvent (composed of terpineol, butyl carbitol, ethyl-cellulose, span 85 and di-*n*-butyl phthalate) to gain the paste which was suitable for screen printing. The paste was printed by screen printing onto the Au interdigital electrode which was preprinted on the alumina substrate, and the thickness of each film was 10 μm which could be controlled by the screen printing machine. To obtain the photoelectric responses of different ingredient points, 66 devices corresponding to the 66 ingredient points were fabricated, which were convenient for photoelectric property measurement. The more details of device preparation could refer to our previous study.[15]

2.3. Photoelectric Property Testing and Characterization of Devices. To evaluate the separation ability of photoexcited electron−hole pairs in the semiconductor materials, photoelectric property measurement was used to assess the photoelectric response capability of the composite material. The photocurrent of each device in the material library was measured under different light sources and bias voltages through a high-throughput screening platform developed by our laboratory.[15] Instantaneous current was acquired by LabVIEW with the data acquisition card (PCI-6225, National Instrument Co.) in real time. The current data of 16 devices could be gotten at one time, and the test current range of the platform was 10^{-8}−10^{-3} A. Three different LED array light sources (Shenzhen Ti-Times Co.) were used; they were ultraviolet (365 nm, 36 W/m^2), blue (475 nm, 80 W/m^2), and green (525 nm, 130 W/m^2). Applied bias voltages were 0.2 V, 0.5 V, 1 V, 2 V, 5 V, and 10 V, respectively. The photocurrent−time curve of pure ZnO under illumination of UV LED at 0.2 V bias is shown in Figure 1. The testing processes was as follows. The bias voltage was loaded at 15 s; at 30 s, the light source was on; at 300 s, the light source was off; at 580 s, the bias voltage was unloaded. The bias voltage from 15 to 580 s was to force the free carriers to move directionally to the electrodes to form current. The current from 15 to 30 s was dark current. From 30 to 300 s, the device was under illumination; thus the photoexcited electron−hole pairs were generated. The photocurrent amplitude at 300 s was adopted as a performance parameter to assess the photoelectric response of the material. From 300 to 580 s, the test current descended with the recombination of the photogenerated carriers inside the material after the light irradiation was off. From 580 to 600 s, the bias

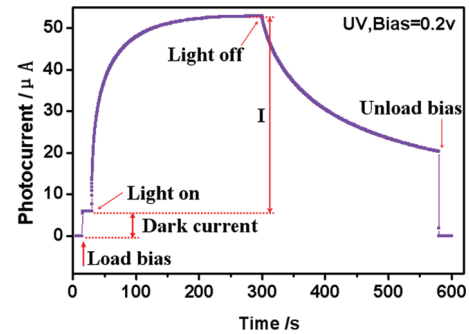

Figure 1. Photocurrent−time test curve of pure ZnO under ultraviolet LED (365 nm, 36 W/m^2) illumination at 0.2 V bias in dry air (20%RH) at room temperature (298 K).

voltage was unloaded, so no current was detected. The testing processes of other devices were in accordance with Figure 1.

X-ray diffractometer (X'Pert PROPANalytical B.V.) was used to analyze the crystal structures of all ingredient points applying graphite monochromatic with Cu Kα1 radiation in the 2θ range from 20 to 80°. The morphology and grain size of the composite were observed through field emission scanning electron microscopy (Hitachi S-4800 FE-SEM).

3. Results and Discussion

3.1. Definition of Composition Effect. As a reference criterion for the evaluation of the composition effect of the composite material, the quantitative formula of the composition effect (*CE*) was provided:

$$CE = \frac{I}{\sum C_i \cdot I_i} \quad (1)$$

Where, I is the performance parameter of the composite, C_i is the percentage of phase i in the composite which can be assayed by all kinds of analysis methods. In this paper, C_i was estimated by the following semiquantitative formula:

$$C_i = \frac{H_i}{\sum H_i} \times 100\% \quad (2)$$

Where, H_i denotes the strongest characteristic peak intensity of phase i of some ingredient point from the XRD pattern, $\sum H_i$ represents the sum of the strongest characteristic peak intensities of all phases of the corresponding ingredient point from the XRD pattern, I_i is the performance parameter of phase i, $C_i \cdot I_i$ is the intrinsic contribution of phase i to the performance of the composite, $\sum C_i \cdot I_i$ is the sum of the intrinsic contribution of all phases to the performance of the composite. We define the specific value of the numerator/denominator as composition effect, and abbreviate it as *CE*. There is a certain range for the value of *CE* in this formula: If $0 < CE < 1$, the composite weakens the performance of the matrixes. The smaller the *CE*, the more obvious effect it weakens. If $CE = 1$, the composite does not change the performance of the matrixes obviously. If $CE > 1$, the composite enhances the performance of the matrixes. The greater the *CE*, the more obvious effect it enhances.

Generally speaking, enhanced composition effect is desired and weakened composition effect should be avoided. The desired composition effect can be achieved through the choice of materials and the fabrication processes.

3.2. Photoelectric Response and Composition Effect of TiO_2/ZnO Composite. The percentage of each phase of TiO_2/ZnO composite was reckoned according to formula 2. For example, for ingredient point 3 in Table 1, the percentage of ZnO phase $C_{ZnO} = (H_Z)/(H_A + H_R + H_Z + H_{ZT}) \times 100\%$; where H_A, H_R, H_Z, and H_{ZT} denote the strongest characteristic peak intensity of anatase TiO_2, rutile TiO_2, ZnO, and $ZnTiO_3$ phase, respectively, from the XRD pattern of ingredient point 3. The percentage of each phase of TiO_2/ZnO composite is shown in Figure 2. Anatase TiO_2 and rutile TiO_2 phase decreases and ZnO phase increases with X_{ZnO} increasing form 0 to 1. Some ingredient points emerged hexagonal $ZnTiO_3$. Herein, X_{ZnO} denotes the mole fraction of ZnO in TiO_2/ZnO composite. X_i was used to describe the different ingredient points conveniently, and it was distinguished from the phase percentage C_i to avoid misunderstanding.

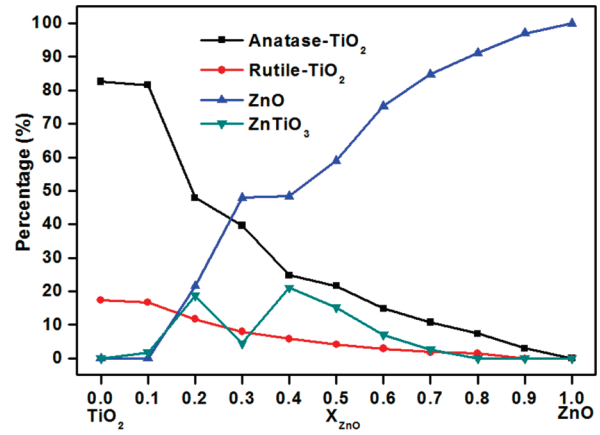

Figure 2. Percentage of each phase of TiO_2/ZnO composite.

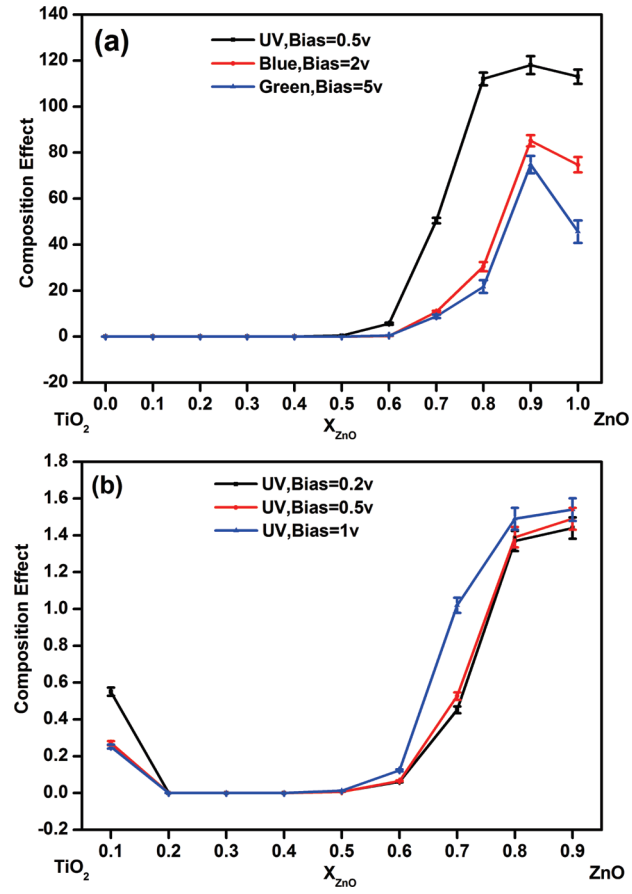

Figure 3. (a) Photocurrent under ultraviolet LED (365 nm, 36 W/m^2) illumination at 0.5 V bias, blue LED (475 nm, 80 W/m^2) illumination at 2 V bias, and green LED (525 nm, 130 W/m^2) illumination at 5 V bias and (b): The composition effect under ultraviolet LED (365 nm, 36 W/m^2) illumination at the bias of 0.2 V, 0.5 V, and 1 V of TiO_2/ZnO composite. Test environment: room temperature (298 K), humidity (20%RH). Each ingredient point corresponded with a device. The devices were prepared through screen printing and sintering at 500 °C for 2 h.

It can be seen from Figure 3a that the photoelectric response of TiO_2 was much less than that of ZnO under the same light source and bias voltage. The probable reasons

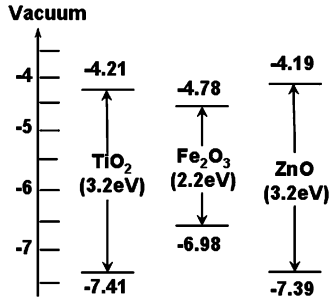

Figure 4. Schematic diagram for the relative position of the vacuum level of TiO_2, ZnO and Fe_2O_3.

were as follows. (1) The light absorption coefficient of TiO_2 (between 1 and 10^3 cm^{-1}) is lower than that of ZnO (between 10^4 and 10^6 cm^{-1}).[17] (2) The quantum efficiency of TiO_2 (3.2%) is less than that of ZnO (33%).[18,19] (3) The carrier mobility of TiO_2 (0.1 $cm^2/(V \cdot s)$) is smaller than that of ZnO (239 $cm^2/(V \cdot s)$).[20,21]

We defined the composition effect of TiO_2/ZnO composite in terms of formula 1:

$$CE = \frac{I}{(C_A + C_R)\cdot I_{TiO_2} + C_Z \cdot I_{ZnO}} \quad (3)$$

Where, I is the photoelectric response of some ingredient point of the composite, in concrete, the value of I is the photocurrent amplitude at 300 s of the device under some LED illumination at a certain bias, which is described in Figure 1. C_A, C_R, and C_Z denote the percentage of anatase TiO_2, rutile TiO_2, and ZnO phase, respectively, of the corresponding ingredient point. I_{TiO_2} and I_{ZnO} refers to the photoelectric response of pure TiO_2 and ZnO under the same conditions, respectively.

The relative position of the energy level of TiO_2/ZnO composite was schematized in Figure 4.[16] The conduction band of ZnO is slightly higher than that of TiO_2; therefore, photogenerated electrons of the conduction band of ZnO can transfer to that of TiO_2. The valence band of TiO_2 is a little lower than that of ZnO; hence, photogenerated holes of the valence band of TiO_2 can migrate to that of ZnO. Such transfer of photoexcited electron−hole pairs could achieve effective separation of photoexcited charges in the photo-induced excitation state and reduced the recombination rate significantly within the TiO_2/ZnO composite.[22] As is reported that TiO_2/ZnO composite increased the surface defects and oxygen vacancies of the particles which could become capture centers of photogenerated electrons, which could inhibit the recombination of photogenerated electron−hole pairs in the composite effectively.[23,24] From the above analysis, the photoelectric response of the composite at all ingredient points should be higher than that of pure TiO_2 and ZnO; in other words, all the ingredient points in the composite should achieve an enhanced composition effect. However, we found that the photoelectric response of the composite was not greater than that of pure TiO_2 and ZnO (Figure 3a), and the composite did not realize elevated composition effect at all ingredient points (Figure 3b). As can be seen from Figure 3a, the device with $X_{ZnO} = 0.9$ under UV, blue, and green light and the device with $X_{ZnO} = 0.8$ under UV light of TiO_2/ZnO composite showed larger photoelectric response than that of pure TiO_2 and ZnO, but other devices with different X_{ZnO} appeared lower in photoelectric response than that of pure TiO_2 and ZnO. The results under other experiment light sources and bias voltages displayed an analogous tendency to that of Figure 3a. Device with $X_{ZnO} = 0.9$ and device with $X_{ZnO} = 0.8$ of TiO_2/ZnO composite under UV light showed *CE* greater than 1; however, other devices with different X_{ZnO} displayed *CE* less than 1 (Figure 3b). The curves of *CE* values under other experiment light sources and bias voltages were approximate to that of Figure 3b. Therefore, in addition to band structure, surface defects and oxygen vacancies, there must be other factors that influence the photoelectric response and the composition effect of the composite. We consider that the intrinsic properties of the materials and the contact state among particles are also key element for the properties of the composite. As is illustrated in Figure 5, the gray round spots stand for TiO_2 particles, and the red ones stand for ZnO particles. As we all know, the carrier mobility of ZnO is higher than that of TiO_2. When the percentage of ZnO was much less than that of TiO_2, unimpeded conduction passageway could not form among ZnO particles (Figure 5a). Generated electron−hole pairs could not transport effectively to the opposite electrodes before recombination, thus the photocurrent detected by the external circuit was in a lower level. Therefore, the low photoelectric response and weakened composition effect with *CE* less than 1 appeared. When the percentage of ZnO which was with high carrier mobility was more than that of TiO_2, unimpeded conduction passageway formed among ZnO particles (Figure 5b). The generated electron−hole pairs could transport effectively to the opposite electrodes before recombination; hence, the photocurrent detected by the external circuit was in a higher level. As a result, it appeared high photoelectric response and enhanced composition effect with *CE* greater than 1. The SEM photographs of different ingredient points are shown in Figure 6. From the SEM images, we can see that the smaller particles are about 30 nm, and the bigger particles are about 100 nm, with no growth compared with as received raw material, and they were well-distributed. Therefore we can hold that the smaller particles are TiO_2 and the bigger particles are ZnO. For ingredient point with $X_{ZnO} = 0.1$ (Figure 6a), a small quantity of ZnO particles distributed among TiO_2 particles; consequently, an unimpeded conduction passageway did not form among the ZnO particles. As for ingredient point with $X_{ZnO} = 0.9$ (Figure 6b), TiO_2 particles distributed in the interstitial site of the ZnO particles which were relatively numerous; as a result, an unimpeded conduction passageway for carrier transporting formed. The

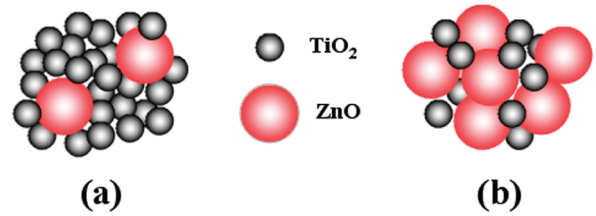

Figure 5. Schematic diagram illustrating the contact state among particles of the TiO_2/ZnO composite.

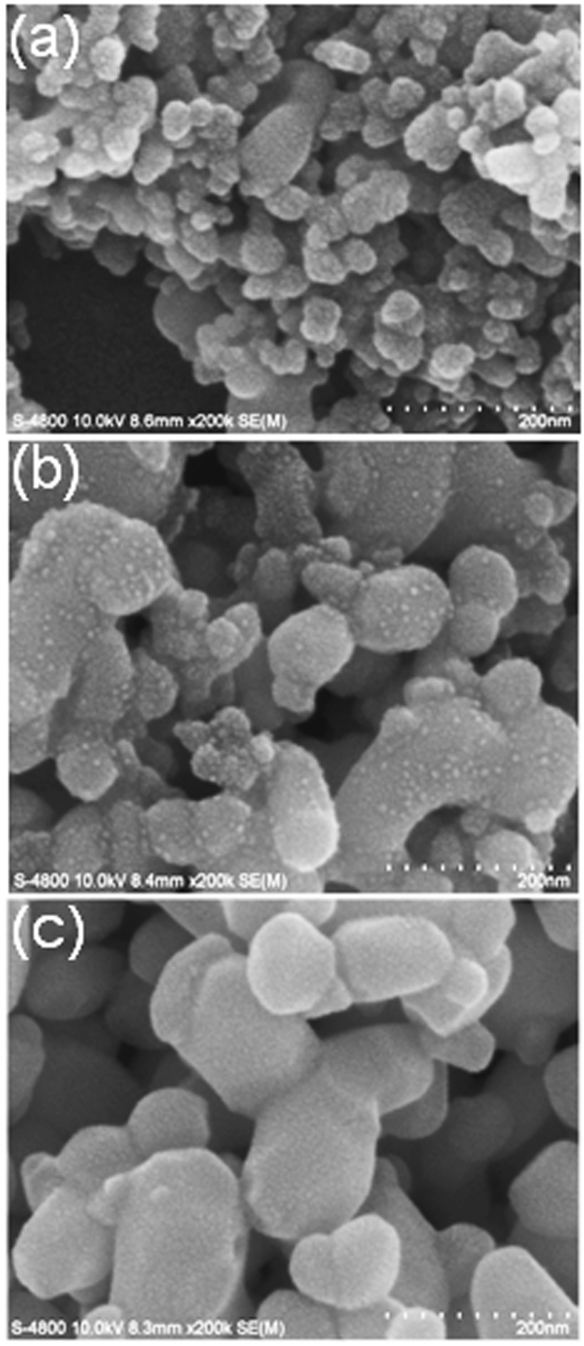

Figure 6. SEM photographs of different ingredient points: (a) X_{ZnO} = 0.1 (TiO_2:ZnO:Fe_2O_3 = 9:1:0), (b) X_{ZnO} = 0.9 (TiO_2:ZnO:Fe_2O_3 = 1:9:0), (c) pure ZnO (TiO_2:ZnO:Fe_2O_3 = 0:10:0).

contact states among particles revealed from the SEM photographs were potent evidence to the above illustration of Figure 5.

3.3. Photoelectric Response and Composition Effect of Fe_2O_3/ZnO and Fe_2O_3/TiO_2 Composite. The photoelectric response of Fe_2O_3 under all experiment light sources and bias voltages was close to the floor level of the test current range of the photoelectric testing platform. The band gap of Fe_2O_3 is 2.2 eV; theoretically it can be excited to generate electron−hole pairs under light less than the wavelength of 560 nm; however, the carrier mobility of Fe_2O_3 is low (0.1 $cm^2/(V \cdot s)$),[25,26] and generated electron−hole pairs recombined extremely easily, so that they had recombined before they reached the opposite electrodes; thus no obvious

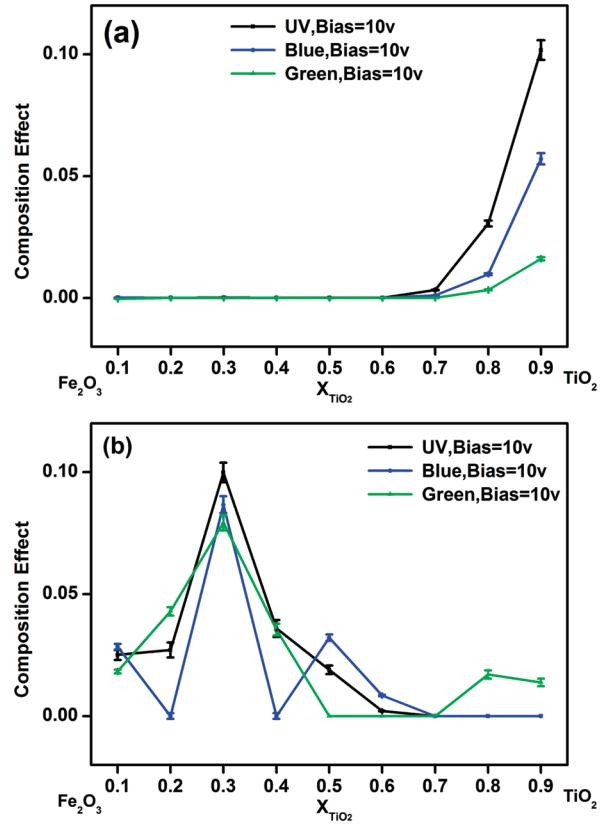

Figure 7. Composition effect of (a) Fe_2O_3/ZnO composite and (b) Fe_2O_3/TiO_2 composite under ultraviolet LED (365 nm, 36 W/m^2), blue LED (475 nm, 80 W/m^2), and green LED (525 nm, 130 W/m^2) illumination at 10 V bias.

photocurrent can be detected. The percentage of each phase of Fe_2O_3/ZnO and Fe_2O_3/TiO_2 composite was calculated through formula 2, and the composition effect of the composite was obtained in terms of formula 1. The *CE* of Fe_2O_3/ZnO and Fe_2O_3/TiO_2 composite under all experiment light sources at 10 V bias voltage was displayed in Figure 7. The test value of *I* was very small, so it showed weakened composition effect with *CE* close to 0. The curves of *CE* value under other experiment light sources and the bias voltages were similar to that of Figure 7. Addition of a small amount of Fe_2O_3 largely weakened the photoelectric response of ZnO and TiO_2. The more amount of Fe_2O_3, the more weakened composition effect it demonstrated. The reason may be that the band gap of Fe_2O_3 is relatively narrow (Figure 4), as a result, electron−hole pairs have recombined through Fe_2O_3 before they reach the opposite electrodes. For this reason, Fe_2O_3/ZnO and Fe_2O_3/TiO_2 composite did not show enhanced composition effect. As can be seen from Figure 4, the energy levels of Fe_2O_3 are between the energy levels of ZnO and TiO_2. We tentatively can conclude that a narrow band gap semiconductor like Fe_2O_3 and broad band gap semiconductors like ZnO and TiO_2 could not constitute the desired composite material which are fit for the strengthened composition effect of the photoelectric property.

3.4. Photoelectric Response and Composition Effect of TiO_2/ZnO/Fe_2O_3 Composite. The photoelectric responses of 66 devices were obtained under different light sources and bias voltages through a high-throughput photoelectric testing platform. The photoelectric responses of all the 66

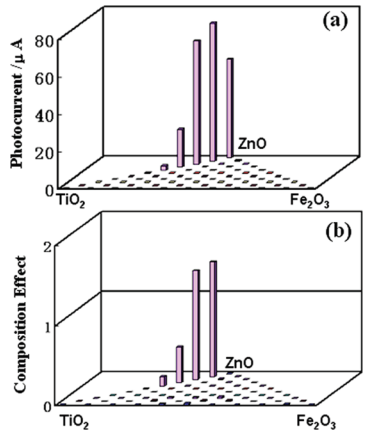

Figure 8. (a) Photocurrent mapping and (b) the composition effect mapping of the different mole ratio of $TiO_2/ZnO/Fe_2O_3$ composite under ultraviolet LED (365 nm, 36 W/m^2) illumination at 0.2 V bias. Test environment: room temperature (298 K), humidity (20% RH). Each ingredient point corresponded with a device. The devices were prepared through screen printing and sintering at 500 °C for 2 h.

devices under ultraviolet at 0.2 V bias voltage are showed in Figure 8a. As can be seen from Figure 8a, the largest photocurrent was obtained when the mole ratio of TiO_2:ZnO:Fe_2O_3 was 1:9:0 in the composite. Besides the TiO_2/ZnO composite, other devices showed a certain level of photoelectric responses, but, they were far less than that of TiO_2/ZnO composite; so, the performances of other devices were not obvious in the map. The maps under other experiment light sources and bias voltages expressed the similar tendency to that of Figure 8a. The obtaining of the composition effect of $TiO_2/ZnO/Fe_2O_3$ composite could refer to formulas 1 and 2. The device with the mole ratio of TiO_2:ZnO:Fe_2O_3 = 1:9:0 in the composite under UV light at 0.2 V bias voltage displayed *CE* greater than 1, and other devices with a different mole ratio from TiO_2:ZnO:Fe_2O_3 showed *CE* less than 1 (Figure 8b). The maps of *CE* value under other experiment light sources and bias voltages were similar to that of Figure 8b. We can conclude that not all the ingredient points displayed the enhanced composition effect in the TiO_2/ZnO/Fe_2O_3 composite. In fact, only a few ingredient points demonstrated positive composition effect; a majority of ingredient points showed weakened composition effect. This is significant for the design of the composite for photocatalytic degradation of pollutants. This is also of great significance for other composite material.

4. Conclusions

On the basis of combinatorial and the idea of equilateral ingredient triangle, a $TiO_2/ZnO/Fe_2O_3$ composite system consisting of 66 ingredient points was designed. The photocurrents under different light sources and bias voltages were measured through a high-throughput screening platform. The photocurrent amplitude at 300 s was chosen as a parameter to evaluate the photoelectric response of the composite, and the largest photoelectric response was obtained when the mole ratio of TiO_2:ZnO:Fe_2O_3 was 1:9:0 in the composite. We expect it would show good performance for photodegradation of pollutants; the relevant research will be carried out in the near future.

To assess the composition effect of the composite material, the quantitative formula of the composition effect was provided for the first time. Not all the ingredient points demonstrated the enhanced composition effect in the TiO_2/ZnO/Fe_2O_3 composite. We expect this quantitative formula of composition effect may provide a means for the evaluation of photoelectric properties and photocatalytic properties of the composite; thus, it may guide the design of composite materials for photocatalytic degradation of pollutants. We also expect this quantitative formula of the composition effect will contribute to the design and evaluation of the composite material.

Acknowledgment. This work was supported by the National Basic Research Program of China (Grants 2009CB939705 and 2009CB939702), Nature Science Foundation of China (No. 50927201) and the Opening Research Foundation of State Key Laboratory of Advanced Technology for Materials Synthesis and Processing (Wuhan University of Technology). The authors are also grateful to Analytical and Testing Center of Huazhong University of Science and Technology.

Supporting Information Available. Figure S1 containing the SEM image of Degussa P25. This material is available free of charge via the Internet at http://pubs.acs.org.

References and Notes

(1) Hamal, D. B.; Klabunde, K. J. *J. Colloid Interface Sci.* **2007**, *311*, 514–522.
(2) Inaba, R.; Fukahori, T.; Hamamoto, M.; Ohno, T. *J. Mol. Catal. A: Chem.* **2006**, *260* (1−2), 247–254.
(3) Yamashita, H.; Harada, M.; Misaka, J. *Catal. Today* **2003**, *84* (3−4), 191–196.
(4) Vohra, M. S.; Tanaka, K. *Water Res.* **2003**, *37* (16), 3992–3996.
(5) Palthi, A.; Narayanan, A.; Thakur, M. *J. Macromol. Sci., Pure Appl. Chem.* **2010**, *47* (4), 375–379.
(6) Neppolian, B.; Wang, Q. L.; Yamashita, H.; Choi, H. *Appl. Catal., A* **2007**, *333* (2), 264–271.
(7) Xi, Y. Y.; Zhou, J. Z.; Zhang, Y.; Dong, P.; Cai, C. D.; Huang, H. G.; Lin, Z. H. *Chem. J. Chin. Univ.* **2004**, *25* (12), 2322–2326.
(8) Zhang, X. T.; Cao, Y. A.; Kan, S. H.; Chen, Y. M.; Tang, J.; Jin, H. Y.; Bai, Y. B.; Xiao, L. Z.; Li, T. J.; Li, B. F. *Thin Solid Films* **1998**, *329*, 568–570.
(9) So, W. W.; Kim, K. J.; Moon., S. J. *Int. J. Hydrogen Energy* **2004**, *29* (3), 229–234.
(10) Li, J.; Yao, M. M.; Zhang, Y.; Yang, H. *Surf. Rev. Lett.* **2009**, *16* (2), 315–321.
(11) Xu, Z. Z.; Long, Y. Z.; Kang, S. Z.; Mu, J. *J. Dispersion Sci. Technol.* **2008**, *29* (8), 1150–1152.
(12) Sanders, D.; Simon, U.; Jockel, J.; Heppel, C.; Brinz, T. *J. Comb. Chem.* **2002**, *4* (5), 511–515.
(13) Sanders, D.; Simon, U. *J. Comb. Chem.* **2007**, *9*, 53–61.
(14) Dai, Q. X.; Xiao, H. Y.; Li, W. S.; Na, Y. Q.; Zhou, X. P. *J. Comb. Chem.* **2005**, *7* (4), 539–545.
(15) Zou, Z. J.; Liu, Y.; Li, H. Y.; Liao, Y. C.; Xie, C. S. *J. Comb. Chem.* **2010**, *12*, 363–369.
(16) Xu, Y.; Schoonen, M. A. A. *Am. Mineral.* **2000**, *85* (3−4), 543–556.
(17) Liu, E. K.; Zhu, B. S.; Luo, J. S. *Semiconductor Physics*, 7th ed.; Publishing House of Electronics Industry: Bei Jing, 2008; p 320.
(18) Wang, C.-Y.; Pagel, R.; Bahnemann, D. W.; Dohrmann, J. K. *J. Phys. Chem. B* **2004**, *108*, 14082–14092.
(19) Al-Suleiman, M. A. M.; Bakin, A.; Waag, A. *J. Appl. Phys.* **2009**, *106* (6), 063111.

(20) Tamaki, Y.; Hara, K.; Katoh, R.; Tachiya, M.; Furube, A. *J. Phys. Chem. C* **2009**, *113* (27), 11741–11746.
(21) Lin, W. W.; Chen, D. G.; Zhang, J. Y.; Lin, Z.; Huang, J. K.; Wang, Y. H.; Huang, F.; Li, W. *Cryst. Growth Des.* **2009**, *9* (10), 4378–4383.
(22) Li, Q. J.; Liu, B. B.; Wang, L.; Li, D. M.; Liu, R.; Zou, B.; Cui, T.; Zou, G. T.; Meng, Y.; Mao, H. K.; Liu, Z. X.; Liu, J.; Li, J. X. *Mater. Chem. Phys.* **2010**, *121*, 432–439.
(23) Sun, R.-D.; Nakajima, A.; Fujishima, A.; Watanabe, T.; Hashimoto, K. *J. Phys. Chem. B* **2001**, *105*, 1984–1990.
(24) Law, M.; Greene, L.; Radenovic, A.; Kuykendall, T.; Liphardt, J.; Yang, P. *J. Phys. Chem. B* **2006**, *110*, 22652–22663.
(25) Hahn, N. T.; H. C. Ye; Ye, H. C.; Flaherty, D. W.; Bard, A. J.; Mullins, C. B. *ACS Nano.* **2010**, *4* (4), 1977–1986.
(26) Guan, Z. D.; Zhang, Z. T.; Jiao, J. S. *Physical Properties of Inorganic Material*; Tsinghua University Publishing House: Bei Jing, 1992; p 233.

CC100121D